# Thermal Properties of Ultrathin Hafnium Oxide Gate Dielectric Films

Matthew A. Panzer, Michael Shandalov, Jeremy A. Rowlette, Yasuhiro Oshima, Yi Wei Chen, Paul C. McIntyre, and Kenneth E. Goodson

***Abstract*—Thin-film $HfO_2$ is a promising gate dielectric material that will influence thermal conduction in modern transistors. This letter reports the temperature dependence of the intrinsic thermal conductivity and interface resistances of 56–200-Å-thick $HfO_2$ films. A picosecond pump–probe thermoreflectance technique yields room-temperature intrinsic thermal conductivity values between 0.49 and 0.95 $W/(m \cdot K)$. The intrinsic thermal conductivity and interface resistance depend strongly on the film-thickness-dependent microstructure.**

***Index Terms*—Hafnium oxide, thermal conductivity, thermal interface resistance, picosecond pump–probe thermometry.**

## I. Introduction

THE THERMAL properties of $HfO_2$, which is currently replacing $SiO_2$ as the gate dielectric of choice below the 45-nm node [1], [2], are of increasing importance since the thermal conductivity and thermal interface resistance can significantly influence the phonon temperature during device switching and indirectly affect device performance and reliability [3], [4]. However, to date, most research has focused almost exclusively on the electrical [5], [6] and chemical interface [7], [8] properties of $HfO_2$. While the previous $3\omega$ measurements of the thermal conductivity of thick ($> 500$ nm) microcrystalline $HfO_2$ films report a room-temperature value of 1.2 $W \cdot m^{-1} \cdot K^{-1}$ [9], recent scanning thermal microscopy measurements of 3-nm-thick a-$HfO_2$ films report a significantly lower value in the range 0.27–0.49 $W \cdot m^{-1} \cdot K^{-1}$ [10]. This strong reduction in conductivity for thin amorphous films can be due to a variety of effects, including contributions from interfaces and variations in volumetric and interface microstructure on thermal conduction. In this letter, we report the intrinsic thermal conductivity and interface resistance of 200-, 118-, and 56-Å-thick $HfO_2$ films grown on Si substrates measured over the temperature range 300 K–500 K using pump–probe time-domain thermoreflectance (TDTR) thermometry.

Manuscript received September 3, 2009; revised September 11, 2009. First published October 30, 2009; current version published November 20, 2009. This work was supported in part by the Semiconductor Research Corporation, by the MARCO Interconnect Focus Center, by the Defense University Research Instrument Program, by the Stanford Graduate Fellowship, and by the Stanford Initiative in Nanoscale Materials and Processes. The review of this letter was arranged by Editor L. Selmi.

M. A. Panzer, J. A. Rowlette, and K. E. Goodson are with the Mechanical Engineering Department, Stanford University, Stanford, CA 94305 USA (e-mail: mpanzer@stanford.edu; rowlette@stanford.edu; goodson@stanford.edu).

M. Shandalov, Y. Oshima, Y. W. Chen, and P. C. McIntyre are with the Material Science and Engineering Department, Stanford University, Stanford, CA 94305 USA (e-mail: michash@stanford.edu; yoshima73@gmail.com; chenyw@stanford.edu; pcm1@stanf.ord.edu).

Color versions of one or more of the figures in this letter are available online at http://ieeexplore.ieee.org.

Digital Object Identifier 10.1109/LED.2009.2032937

## II. Sample Fabrication and Experimental Setup

The samples were prepared by cleaning prime Si (100) wafers (1–10 $\Omega \cdot$ cm) by the RCA method [11], followed by immediate oxidation for 45 s in a slot-plane-antenna plasma processing chamber at 500 °C and 4-kW microwave power in a 5-torr ambient with $O_2$ flow rate of 400 sccm and Ar flow rate of 1200 sccm. The thickness of the plasma $SiO_2$ was measured to be 1.7 nm by ellipsometry. Different thicknesses of $HfO_2$ were subsequently deposited onto the samples by controlling the number of cycles in the atomic-layer-deposition (ALD) method, described elsewhere [12], at 250 °C with tetrakisdethylamino hafnium (TDMAHf) as the precursor and water as the oxidant. Following the $HfO_2$ ALD, 30 nm of Al was deposited by e-beam evaporation without substrate heating. Finally, the samples were annealed in forming gas (95% $N_2$ and 5% $H_2$) at 400 °C for 30 min.

Transmission electron microscopy (TEM) imaging and selective area electron diffraction (SAED) analysis of the samples after metallization and annealing reveal that the a-$HfO_2$ films contain increasing volume fractions of tetragonal (t-$HfO_2$) nanocrystals with increasing film thickness. Fig. 1(a) shows a representative sample cross section of the 200-Å-thick $HfO_2$, showing embedded nanoscale t-$HfO_2$ grains. The plan-view TEM images of the 200 and 118 Å in Fig. 1(b) and (c) demonstrate an increase in crystallite volume fraction with film thickness. Table I summarizes the TEM measurements of the film thicknesses and composition, including crystalline volume fraction estimations extracted from large field-of-view TEM images (not shown). The comparison of cross-sectional TEMs of regions with and without aluminum suggests that oxygen is transferred from the underlying layers to form an amorphous $AlO_x$ interfacial layer at the $HfO_2/Al$ interface during the anneal process, likely from residual oxidant species present in the as-grown ALD $HfO_2$ [13], and for thinner $HfO_2$ layers, from the $SiO_2$ interlayer via a previously reported oxygen gettering phenomenon [14].

Picosecond TDTR is an established technique for measuring the thermal conductivity and interface resistances in thin films, thoroughly described in the literature [15]–[17]. In brief, periodic picosecond pump pulses from a mode-locked Nd:$YVO_4$ laser (9.2 ps pulse width, 82 MHz repetition rate, ~10 nJ/pulse energy, 1064 nm wavelength) deposit heat in the metal film, establishing a transient temperature field within the sample. The surface temperature of the metal is then measured by an optically delayed probe beam, derived from the pump, which is reflected off of the sample and collected by a fast photodetector. The pump beam is externally modulated at 8 MHz for lock-in detection and converted to 532 nm with a second harmonic

0741-3106/$26.00 © 2009 IEEE

Authorized licensed use limited to: Stanford University. Downloaded on April 15,2010 at 02:18:47 UTC from IEEE Xplore. Restrictions apply.

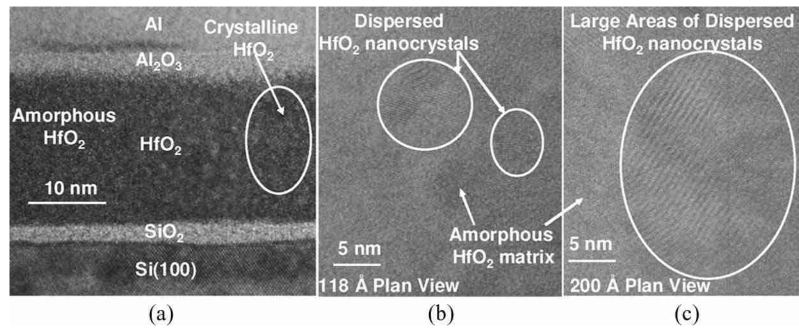


Fig. 1. (a) Representative cross-sectional TEM of 200-Å-thick sample showing $HfO_2$ nanocrystals embedded in an amorphous $HfO_2$ matrix. (b) Plan view of the 118-Å sample showing a low density of $HfO_2$ nanoparticles in an amorphous matrix. (c) Plan view of the 200-Å sample showing a high density of $HfO_2$ crystallites in an amorphous matrix.

TABLE I
STRUCTURE AND COMPOSITION OF SAMPLE FILMS

| $HfO_2$ Thickness (Å) (±10) | Al Thickness (Å) (±20) | $SiO_2$ Thickness (Å) | a-$Al_2O_3$ Thickness (Å) | Crystal Fraction in a-$HfO_2$ | Effective (intrinsic) Film Thermal Conductivity at 400 K from (1). ($Wm^{-1}K^{-1}$) |
|---|---|---|---|---|---|
| 200 | 390 | 15 | 18 | 20-30 % | 0.68 (0.80) |
| 118 | 330 | 15 | 16 | 5-10 % | 0.54 (1.14) |
| 56 | 410 | Absent | 14 | Absent | 0.42 (0.58) |

generator to enable the rejection of pump leakage at the detector. The coaligned pump and probe beams are focused on the sample surface with Gaussian waist diameters of 10.0 and 5.0 $\mu$m and powers of 20 and 5 mW, respectively. The temperature excursion ($< 10$ K) due to the laser heating is significantly less than the $HfO_2$ deposition temperature.

The thermal conductivity and buried interface resistances are extracted by fitting the data to the solution of the radial–symmetric 3-D heat diffusion equation for the multilayer stack with surface heating by a modulated periodic pulse train [15], [17]. The measurement system and thermal model were validated by confirming a measured value of 1.4 $W \cdot m^{-1} \cdot K^{-1}$ for the thermal conductivity of a 102-nm-thick thermally grown $SiO_2$ film coated with a 38-nm-thick Al film. The unique temporal dependence of the thermal response sensitivity on the spatial distribution of thermal properties permits their isolation [17], [18]. We fit the data with two parameters: the $HfO_2$ thermal conductivity $k_{HfO_2}$ and the total $HfO_2-SiO_2-Si$ boundary resistance $R_b$. In fitting $k_{HfO_2}$ and $R_b$, we set the $HfO_2-Al$ interface resistance to zero, as the data bound the value to below 3 $m^2K/GW$, below which data extraction is insensitive to its value. The $HfO_2$ heat capacity and other required thermal properties were taken from the literature [19].

## III. RESULTS AND DISCUSSION

Fig. 2 shows the intrinsic $k_{HfO_2}$ and $R_b$ temperature dependence, with the volumetric $SiO_2$ resistance subtracted, assuming 1.4 $W/(m \cdot K)$ for the $SiO_2$ thermal conductivity. The uncertainty bars in Fig. 1 include the effects of the film thickness uncertainty in Table I, the contribution of the $Al_2O_3$ layer and $HfO_2-Al$ interface, and the uncertainty related to the ability of the measurement to uniquely resolve the interface and volumetric resistances. The latter is the dominant uncertainty in the 56-Å film data. Fitting these data with a single effective conductivity parameter provides the conductivity uncertainty lower bound. The thermal conductivities of the 118- and 56-Å samples both exhibit slight increases with temperature, a characteristic of amorphous dielectrics consistent with previous measurements [9]. The weaker temperature dependence of the thermal conductivity of the 200-Å sample is most likely due to the offsetting temperature trends for the volumetric resistance contributions of the amorphous and crystalline components. The $k_{HfO_2}$ data fall between the theoretical estimations from the minimum thermal conductivity model [20] $k_{min}$ of $HfO_2$ [Fig. 2(a)] when evaluated using either the atomic or molecular number density in combination with the known $HfO_2$ acoustic velocities [21]. The application of these number density

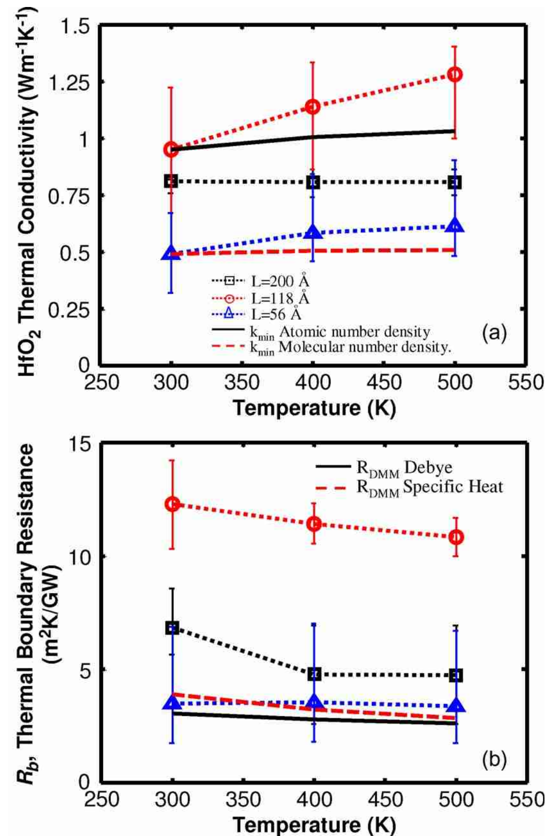


Fig. 2. (a) Intrinsic $HfO_2$ thermal conductivity for (black square) 200 Å, (red circle) 118 Å, and (blue triangle) 56 Å as a function of temperature. Predictions for the minimum thermal conductivity theory calculated using the (solid black) atomic number density and (red dashed) molecular density. (b) Total thermal resistance for the $HfO_2-SiO_2-Si$ interface, and DMM predictions in (solid black) the Debye approximation [25], [26] and (red dashed) using the specific heat correction to the density of states [26].

Authorized licensed use limited to: Stanford University. Downloaded on April 15,2010 at 02:18:47 UTC from IEEE Xplore. Restrictions apply.

definitions is related to the relevant fundamental vibration unit, which is not entirely understood for amorphous materials [22].

Due to its upper bound of 3 $m^2K/GW$, the possible residual $HfO_2-Al$ interface resistance cannot explain the reduction in intrinsic thermal conductivity for the 200-Å film compared to the 118-Å film. This trend may be due to the increased $HfO_2$ nanocrystal volume fraction in the 200-Å film creating additional interface resistances, which can be larger ($\sim$10 $m^2K/GW$) than the reduction in resistance due to the substitution of the crystalline phase. Previous work reported nanolaminate thermal conductivities [23] below the minimum due to the presence of interfaces and similar reductions in the $In_{0.53}Ga_{0.47}As$ thermal conductivity with increasing ErAs nanoparticle concentration due to the scattering of mid-to-long-wavelength phonons [24].

Because $R_b$ and the volumetric resistance $(L/k_{HfO_2})$ are comparable in value, the effective thermal conductivity of the layer will exhibit a thickness dependence according to

$$k_{eff} = \frac{k_{HfO_2}}{1 + R_b k_{HfO_2}/L_{HfO_2}} \quad (1)$$

presented in Table I for a typical device operating temperature of 400 K. Including $R_b$ in $k_{eff}$ yields values closer to the previously measured thin-film values [10].

Currently, there are no rigorous models accurately predicting thermal interface resistances at high temperature ($> 20$ K) [25]; however, the diffuse mismatch model (DMM) is a simplified approach that assumes that phonons are diffusely scattered at an interface, which is an approximation most relevant at room temperature [25], [26]. The reasonable predictions of the DMM model suggest that the interfaces are of high quality and that long-wavelength phonons may be important in heat conduction. The relative values of the interface resistances for the three films are most likely due to the variations in interface quality observed in the TEMs, with the lowest interface resistance for the 56-Å film, which is the most diffused.

## IV. Conclusion

The intrinsic $HfO_2$ thermal conductivity depends on the film thickness and postdeposition processing, deviating from both bulk values and the measurements of effective film thermal conductivities. Consequently, modifications in gate dielectric microstructure due to postdeposition thermal processing can impact device temperatures through the unexpected changes in the thickness-dependent film thermal conductivity.

## References

[1] K. Mistry, C. Allen, C. Auth, B. Beattie, D. Bergstrom, M. Bost, M. Brazier, M. Buehler, A. Cappellani, R. Chau, C. H. Choi, G. Ding, K. Fischer, T. Ghani, R. Grover, W. Han, D. Hanken, M. Hattendorf, J. He, J. Hicks, R. Huessner, D. Ingerly, P. Jain, R. James, L. Jong, S. Joshi, C. Kenyon, K. Kuhn, K. Lee, H. Liu, J. Maiz, B. McLntyre, P. Moon, J. Neirynck, S. Pae, C. Parker, D. Parsons, C. Prasad, L. Pipes, M. Prince, P. Ranade, T. Reynolds, J. Sandford, L. Shifren, J. Sebastian, J. Seiple, D. Simon, S. Sivakumar, P. Smith, C. Thomas, T. Troeger, P. Vandervoorn, S. Williams, and K. Zawadzki, "A 45 nm logic technology with high-$k$ + metal gate transistors, strained silicon, 9 Cu interconnect layers, 193 nm dry patterning, and 100% Pb-free packaging," in *IEDM Tech. Dig.*, 2007, pp. 247–250.

[2] G. D. Wilk, R. M. Wallace, and J. M. Anthony, "High-$\kappa$ gate dielectrics: Current status and materials properties considerations," *J. Appl. Phys.*, vol. 89, no. 10, pp. 5243–5275, May 2001.

[3] E. Pop and K. E. Goodson, "Thermal phenomena in nanoscale transistors," *J. Electron. Packag.*, vol. 128, no. 2, pp. 102–108, Jun. 2006.

[4] E. Pop, S. Sinha, and K. E. Goodson, "Heat generation and transport in nanometer-scale transistors," *Proc. IEEE*, vol. 94, no. 8, pp. 1587–1601, Aug. 2006.

[5] H. Kim, P. C. McIntyre, and K. C. Saraswat, "Effects of crystallization on the electrical properties of ultrathin $HfO_2$ dielectrics grown by atomic layer deposition," *App. Phys. Lett.*, vol. 82, no. 1, pp. 106–108, Jan. 2003.

[6] Z. Xu, M. Houssa, R. Carter, M. Naili, S. De Gendt, and M. Heyns, "Constant voltage stress induced degradation in $HfO_2/SiO_2$ gate dielectric stacks," *J. Appl. Phys.*, vol. 91, no. 12, pp. 10 127–10 129, Jun. 2002.

[7] R. Jiang, E. Xie, and Z. Wang, "Interfacial chemical structure of $HfO_2/Si$ film fabricated by sputtering," *Appl. Phys. Lett.*, vol. 89, no. 14, pp. 142 907-1–142 907-3, Oct. 2006.

[8] O. Renault, D. Samour, D. Rouchon, P. Holliger, A. M. Papon, D. Blin, and S. Marthon, "Interface properties of ultra-thin $HfO_2$ films grown by atomic layer deposition on $SiO_2/Si$," *Thin Solid Films*, vol. 428, no. 1/2, pp. 190–194, Mar. 2003.

[9] S. M. Lee, D. G. Cahill, and T. H. Allen, "Thermal conductivity of sputtered oxide films," *Phys. Rev. B, Condens. Matter*, vol. 52, no. 1, pp. 253–257, Jul. 1995.

[10] M. Hinz, O. Marti, B. Gotsmann, M. A. Lantz, and U. Durig, "High resolution vacuum scanning thermal microscopy of $HfO_2$ and $SiO_2$," *Appl. Phys. Lett.*, vol. 92, no. 4, pp. 043 122-1–043 122-3, Jan. 2008.

[11] J. D. Plummer, M. D. Deal, and P. B. Griffin, *Silicon VLSI Technology—Fundamentals, Practice and Modeling*. Englewood Cliffs, NJ: Prentice-Hall, 2000, p. 159.

[12] T. Sugawara, R. Sreenivasan, and P. C. McIntyre, "Mechanism of germanium plasma nitridation," *J. Vac. Sci. Technol. B, Microelectron. Process. Phenom.*, vol. 24, no. 5, pp. 2442–2448, Sep. 2006.

[13] M. T. Ho, Y. Wang, R. T. Brewer, L. S. Wielunski, Y. J. Chabal, N. Moumen, and M. Boleslawski, "*In situ* infrared spectroscopy of hafnium oxide growth on hydrogen-terminated silicon surfaces by atomic layer deposition," *Appl. Phys. Lett.*, vol. 87, no. 13, pp. 133 103-1–133 103-3, Sep. 2005.

[14] H. Kim, P. C. McIntyre, C. O. Chui, K. C. Saraswat, and S. Stemmer, "Engineering chemically abrupt high-$k$ metal oxide/silicon interfaces using an oxygen-gettering metal overlayer," *J. Appl. Phys.*, vol. 96, no. 6, pp. 3467–3472, Sep. 2004.

[15] D. G. Cahill, "Analysis of heat flow in layered structures for time-domain thermoreflectance," *Rev. Sci. Instrum.*, vol. 75, no. 12, pp. 5119–5122, Nov. 2004.

[16] W. S. Capinski and H. J. Maris, "Improved apparatus for picosecond pump-and-probe optical measurements," *Rev. Sci. Instrum.*, vol. 67, no. 8, pp. 2720–2726, Aug. 1996.

[17] A. Schmidt, M. Chiesa, X. Chen, and G. Chen, "An optical pump–probe technique for measuring the thermal conductivity of liquids," *Rev. Sci. Instrum.*, vol. 79, no. 6, pp. 064 902-1–064 902-5, Jun. 2008.

[18] R. M. Costescu, M. A. Wall, and D. G. Cahill, "Thermal conductance of epitaxial interfaces," *Phys. Rev. B, Condens. Matter*, vol. 67, no. 5, pp. 054 302-1–054 302-5, Feb. 2003.

[19] T. P. R. Center, *Thermophysical Properties of Matter*. La Fayette, IL: Purdue Univ. Press, 1970.

[20] D. G. Cahill, S. K. Watson, and R. O. Pohl, "Lower limit to the thermal conductivity of disordered crystals," *Phys. Rev. B, Condens. Matter*, vol. 46, no. 10, pp. 6131–6140, Sep. 1992.

[21] K. F. M. Ivanda, S. Musić, M. Ristić, M. Gotić, D. Ristić, A. M. Tonejc, I. Djerdj, M. M. M. Mattarelli, F. Rossi, M. Ferrari, A. Chiasera, Y. Jestin, G. C. Righini, W. Kiefer, and R. R. Gonçalves, "Low wavenumber Raman scattering of nanoparticles and nanocomposite materials," *J. Raman Spectrosc.*, vol. 38, no. 6, pp. 647–659, Jun. 2007.

[22] J. J. Freeman and A. C. Anderson, "Thermal conductivity of amorphous solids," *Phys. Rev. B, Condens. Matter*, vol. 34, no. 8, pp. 5684–5690, 1986.

[23] R. M. Costescu, D. G. Cahill, F. H. Fabreguette, Z. A. Sechrist, and S. M. George, "Ultra-low thermal conductivity in W/Al2O3 nanolaminates," *Science*, vol. 303, no. 5660, pp. 989–990, Feb. 2004.

[24] W. Kim, J. Zide, A. Gossard, D. Klenov, S. Stemmer, A. Shakouri, and A. Majumdar, "Thermal conductivity reduction and thermoelectric figure of merit increase by embedding nanoparticles in crystalline semiconductors," *Phys. Rev. Lett.*, vol. 96, no. 4, pp. 045 901-1–045 901-4, Feb. 2006.

[25] E. Schwartz and R. Pohl, "Thermal boundary resistance," *Rev. Mod. Phys.*, vol. 61, no. 3, pp. 605–668, 1989.

[26] P. E. P. Lisa De Bellis and R. S. Prasher, "Variations of acoustic and diffuse mismatch models in predicting thermal-boundary resistance," *J. Thermophys. Heat Transf.*, vol. 14, no. 2, pp. 144–150, 2000.

Authorized licensed use limited to: Stanford University. Downloaded on April 15,2010 at 02:18:47 UTC from IEEE Xplore. Restrictions apply.